Nanoscale

Accepted Manuscript

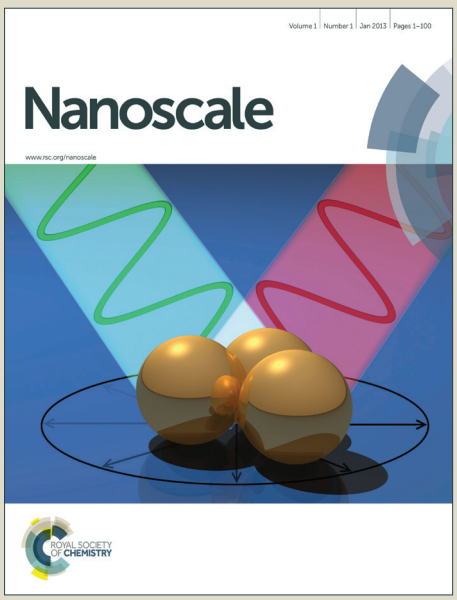

ROYAL SOCIETY OF CHEMISTRY

www.rsc.org/nanoscale

Nanoscale

RSCPublishing

ARTICLE

Hierarchically nanotextured surfaces maintaining superhydrophobicity under severely adverse conditions†

Cite this: DOI: 10.1039/x0xx00000x

Tanmoy Maitra,[a] Carlo Antonini,[a] Matthias Auf der Mauer, [a] Christos Stamatopoulos, [a] Manish K. Tiwari [ζ] and Dimos Poulikakos[a]*

Received 00th January 2012,
Accepted 00th January 2012

DOI: 10.1039/x0xx00000x

www.rsc.org/

Superhydrophobic surfaces are highly desirable for a broad range of technologies and products affecting everyday life. Despite significant progress in recent years in understanding the principles of hydrophobicity, mostly inspired by surface designs found in nature, many man-made surfaces employ readily processable materials, ideal to demonstrate principles, but with little chance of survivability outside a very limited range of well controlled environments. Here we focus on the rational development of robust, hierarchically nanostructured, environmentally friendly, metal–based (aluminum) superhydrophobic surfaces, which maintain their performance under severely adverse conditions. Based on their functionality, we superpose selected hydrophobic layers (i.e. self-assembled monolayers, thin films, or nanofibrous coatings) on hierarchically textured aluminum surfaces, collectively imparting high level robustness of superhydrophobicity under adverse conditions. These surfaces exhibit simultaneously chemical stability, mechanical durability and droplet impalement resistance. They maintained impressively their superhydrophobicity after exposure to severely adverse chemical environments like strong alkaline (pH ~9-10), acidic (pH ~2-3), and ionic solutions (3.5 weight% of sodium chloride), and could simultaneously resist water droplet impalement up to impact velocity of 3.2 m/s as well as withstand standard mechanical durability tests.

Introduction

Superhydrophobic surfaces have been attracting great interest, not only because their design involves exciting multidisciplinary scientific challenges, but also due to their great potential for industrial applications, exemplified by anti-icing,[1,2,3,4,5] anti-fouling,[6] anti-fogging,[7] and anti-corrosion[8] and in promotion of drop wise condensation.[9] Significant progress has been achieved in understanding the principles of hydrophobicity, mostly inspired by surface designs found in nature, ranging from plant leaves to the skin of fish or other swimming organisms,[10, 11] the performance of which is tailored by evolution in their natural environments. However, majority of man-made surfaces employ readily processable albeit sensitive materials, which cannot survive outside a very limited range of well controlled environments, prohibiting their potential usability.

Both surface roughness and chemistry play an important role in superhydrophobicity. A detailed thermodynamic analysis of the role of surface roughness (at the microscale) and surface chemistry in this context has been discussed by Li *et al.*[12] In particular, the combination of nano- and microstructures can be advantageous not only in improving surface non-wetting properties, but also in creating surfaces with enhanced mechanical durability, as discussed in Li *et al.*[13] based on thermodynamic and mechanics principles. Typically, in a first step a micro-, nano- or hierarchical morphology is created followed by a second step involving surface chemistry by coating this morphology with low surface energy molecules. To accomplish the first step, various methods exist, such as electrospinning,[14-18] chemical vapor deposition,[19] hydrothermal processes,[20, 21] chemical etching.[22-37] The techniques vary depending on the substrate on which superhydrophobicity needs to be imparted.[20-22, 26, 34, 35, 38, 39] A prominent exception to the above two step procedure are fluropolymer based superhydrophobic surfaces, where either by texturing the fluoropolymer or by including its particulate forms in the coating superhydrophobicity is obtained in a single step.[3, 40] In addition to a fluropolymer, an intrinsically hydrophobic elastomer, poly(dimethylsiloxane) (PDMS), can be used at the surface if a superhydrophobic property needs to be imparted. A PDMS-based hierarchical superhydrophobic surface was developed by Cortese *et al.*[41], through a multistep process including fabrication of square micropillars by soft lithography, followed by generation of nanoscale roughness by means of CF_4 plasma treatment. Changes in the influence of micro- and nanoscale geometrical structures were investigated to show that surfaces with extreme superhydrophobicity can be achieved.

The ability to impart superhydrophobicity to commonly used metals, such as aluminum, found in a plethora of applications, is highly

Nanoscale

RSCPublishing

ARTICLE

desirable. Fabrication of superhydrophobic surfaces based on aluminum that simply show repellency of a sessile water drop for the purposes of a laboratory demonstration is not a significant challenge any more and the literature contains several such works.[30, 31, 42,43] On the other hand, several scientific and technical challenges need to be overcome on the way to the realization of *multi-functional* and *robust* superhydrophobic surfaces on aluminum, having the potential of employment in adverse environments and realistic applications.

In this work, we focus on developing a rational framework for superhydrophobic textures on aluminum in a scalable manner, aiming at chemical stability, mechanical durability, and high liquid impalement resistance into the texture, as schematically illustrated in Fig. 1. We employ a systematic approach to attain and characterize the chemical stability in multiple environments, with the objective of understanding which design and fabrication approaches, ranging from multi-layer functionalization to multi-scale morphology control, can provide the best performance.

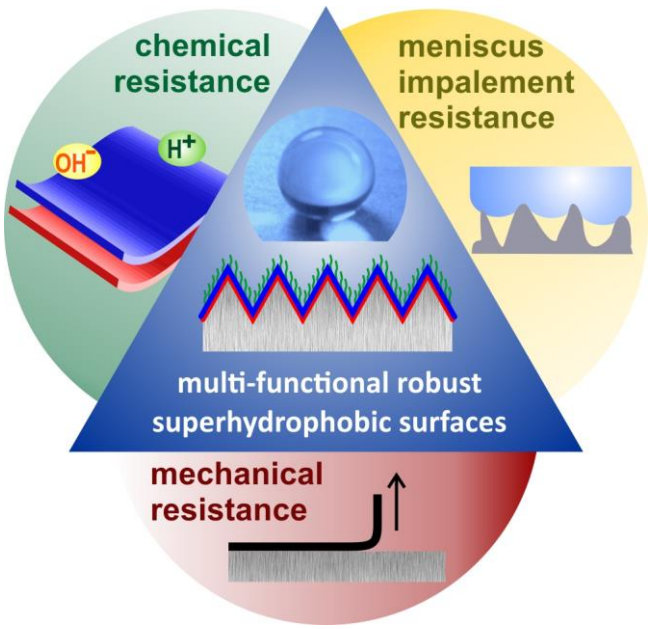

Fig. 1 Challenges for fabrication of multi-functional and robust aluminum based superhydrophobic surfaces.

A critical challenge related to the use of aluminum as substrate for superhydrophobic surfaces is its high reactivity due to its position in the electromotive series, compared to other metals such as zinc, iron, copper, silver etc. The native oxide layer on aluminum, which acts as a protective layer, can be easily dissolved in various chemical environments such as acidic or alkaline water, causing aluminum exposure to corrosion. This poses a serious problem and thus considerable attempts have been made to develop aluminum-based superhydrophobic surfaces with protective layers towards different chemical environments. [8, 29-31, 36, 37, 44-51] Xu *et al.*[45] showed the stability of superhydrophobic surfaces for only 3 to 5 hours in different pH media and in corrosive environment, such as acetic acid-water mixture. Saleema *et al.*[31] also evaluated the stability of superhydrophobic surfaces in corrosive environment like in 3.5 weight% sodium chloride solution, reporting degradation after one day. Similar results were reported by Bo *et al.*[8] However, the development of long-term sustainable superhydrophobic surfaces of potential use in many applications has remained a challenge.

Another critical issue is the development of a scalable and environmentally benign fabrication technique for such superhydrophobic surfaces, which can be applied to large scale processes and applications. Despite a number of previous works attempting to address the scalability issue,[8, 29, 31, 32, 49] the reactive etchant used to enhance surface roughness in these techniques are strongly acidic or basic solutions, which are not well suited from the sustainability perspective.

The second challenge for superhydrophobic surfaces is the resistance to liquid meniscus impalement, e.g. under drop impact, or under high-pressure underwater environments. Impalement should be avoided, since it causes a strong increase in contact angle hysteresis, leading to a reduction of drop mobility[52,53] and causing drops to stick after impact (transition from Cassie-Baxter to Wenzel state), instead of rebounding.[54-56] The property of high impalement resistance can be of great practical relevance, for example to avoid accumulation of rain drops on a surface, in the design of anti-icing surfaces,[57] or in marine applications.

The third challenge is mechanical durability.[49, 58-60] Deng *et al.*[58] demonstrated the fabrication of a thermally and mechanically stable superhydrophobic surface based on glass. In this case, the mechanical stability test was carried out by impacting of sand particles (size of particles ~100-300 µm in diameter) from a certain height. Their fabricated surface showed the loss of superhydrophobic property on impact of sand particles from more than 30 cm distance. In addition, the proposed fabrication process is not up scalable and cannot used for functionalization of aluminum. Cho *et al.*[49] fabricated abrasion resistant aluminum based superhydrophobic surfaces. In their mechanical test, a known load was placed on an abrasion film, which was then placed upon a superhydrophobic surface and the surface was pulled with a velocity of 5 mm/s. With abrasion load of 1000 kg, the hysteresis of a micro/nano hierarchical surface went up to 30°. Although promising, the proposed fabrication process makes use of environmentally adverse alkali solution for the creation of roughness morphology. Xu *et al.*[60] showed a facile method to fabricate a superhydrophobic surface by coating candle soot on glass. The candle soot based superhydrophobic coating was mechanically quite durable and resistant against sand (particle size ~100-300 µm) abrasion tests with

Nanoscale

RSCPublishing

ARTICLE

sand-impacting velocity of ~3 m/s. However, the adhesion of the superhydrophobic coating with the different useful substrates such as metals was not addressed.

To sum up, a rational framework for superhydrophobic surface design for materials with great demand for direct application potential, such as aluminum, also delivering the necessary robustness, from both mechanical and chemical perspective is lacking. To address this issue, the superhydrophobic surface were designed by introducing micro- and nanoscale texturing on aluminum by etching with ferric chloride, since this can be considered an environmental benign chemical and is already widely used for industrial processes.[61] Ferric chloride causes dislocation etching of aluminum[51, 62] and thus helps creating a rough morphology on the aluminum surface. Upon texturing, surface functionalization was achieved using a combination of three different functional coatings. The three functional coatings consisted of a self-assembled molecular monolayer of a fluroalkylsilane (FDTS), a thin film coating of PDMS, and a self-assembly of methyltrichlorosilane (MTS) nanofibers.[63] The underlying thesis was to show that, although surfaces with any of these top layers could be employed to obtain a superhydrophobic surface with high drop repellency and mobility, as it has been shown in previous works referred above, it is a careful combination of all these layers that leads to robustness. Therefore, we first evaluated each layer for robustness individually, and then combined them for optimal performance. The resistance of each superhydrophobic surface after exposure to different harsh environments was systematically investigated to assess chemical stability. To assess resistance to liquid penetration in dynamic conditions and estimate the surface capillary pressure resisting liquid meniscus penetration, drop impact tests were employed. Finally, surface mechanical durability was studied using the ASTM standard adhesive tape test (EN ISO 2409), i.e. a tape peel test.[64] During all the stability/durability studies, the surface degradation was monitored by measuring the advancing and receding contact angles, as well as their difference (contact angle hysteresis) which is essential for correctly predicting both drop capillary adhesion and sticky/rebound behavior after the impact.[65, 66] In addition, a thorough thermodynamic analysis of the contact angle hysteresis by Li *et al.*[67] highlighted the need to understand and predict the contact angle hysteresis for best superhydrophobicity.

Results show that PDMS on the top of the FDTS layer significantly enhances chemical stability and leads to excellent mechanical robustness. On the other hand, the presence of MTS nanofibers on the top of the FDTS and PDMS layers offers a clear advantage in terms of meniscus impalement resistance under dynamic conditions, while preserving good chemical resistance, which could not be achieved by the use of MTS nanofibers alone. In addition, such surface shows also good mechanical properties, resisting approximately 10 cycles of tape peel tests. We also show that for applications where requirements on chemical stability are not stringent, but instead high mechanical durability is required, a different superhydrophobic surface with a microspherulite morphology and coated only with a FDTS monolayer can resist 50 tape peel tests with no signs of degradation ($\Delta\theta < 10°$).

Results and discussion

The processes scheme for superhydrophobic surface fabrication is described in Fig. 2. Overall, three different processes, termed A, B and C, were developed, each consisting of up to four steps. Fig. 2 also includes the representative SEM images below the corresponding schematic. In all three processes, the aluminum surface was etched with 1 M ferric chloride solution. For the A and B processes, the etching temperature was 25°C, whereas for the C process the temperature was 50°C. From the SEM images in Fig. 2, it is clear that two different morphologies were achieved from these two etching conditions: The A1 and B1 surfaces showed sharp pits, which are typical of crystal dislocation etching processes,[62] whereas the C1 surface was populated with rounded microspherulites, which resemble the well-known lotus leaf[68] microstructures on the pit walls, creating a dual-scale hierarchical texturing. Based on the overall scheme in Fig. 2, we terminated the process as needed to obtain superhydrophobic surfaces with different morphologies, i.e. microstructured or hierarchical, and with single or multiple hydrophobic layers, including a self-assembly of FDTS (step #2), the formation of a thin film of PDMS (step #3), and non-woven nanofibers of MTS (step #4). For example, coating A3 refers to an aluminum surface etched at 25°C to obtain the microstructure, followed by functionalization with FDTS and PDMS, where PDMS imparts chemical resistance, and FDTS acts both as a protective layer and also helps improve the adhesion between the aluminum substrate and the PDMS layer.

Nanoscale

RSCPublishing

ARTICLE

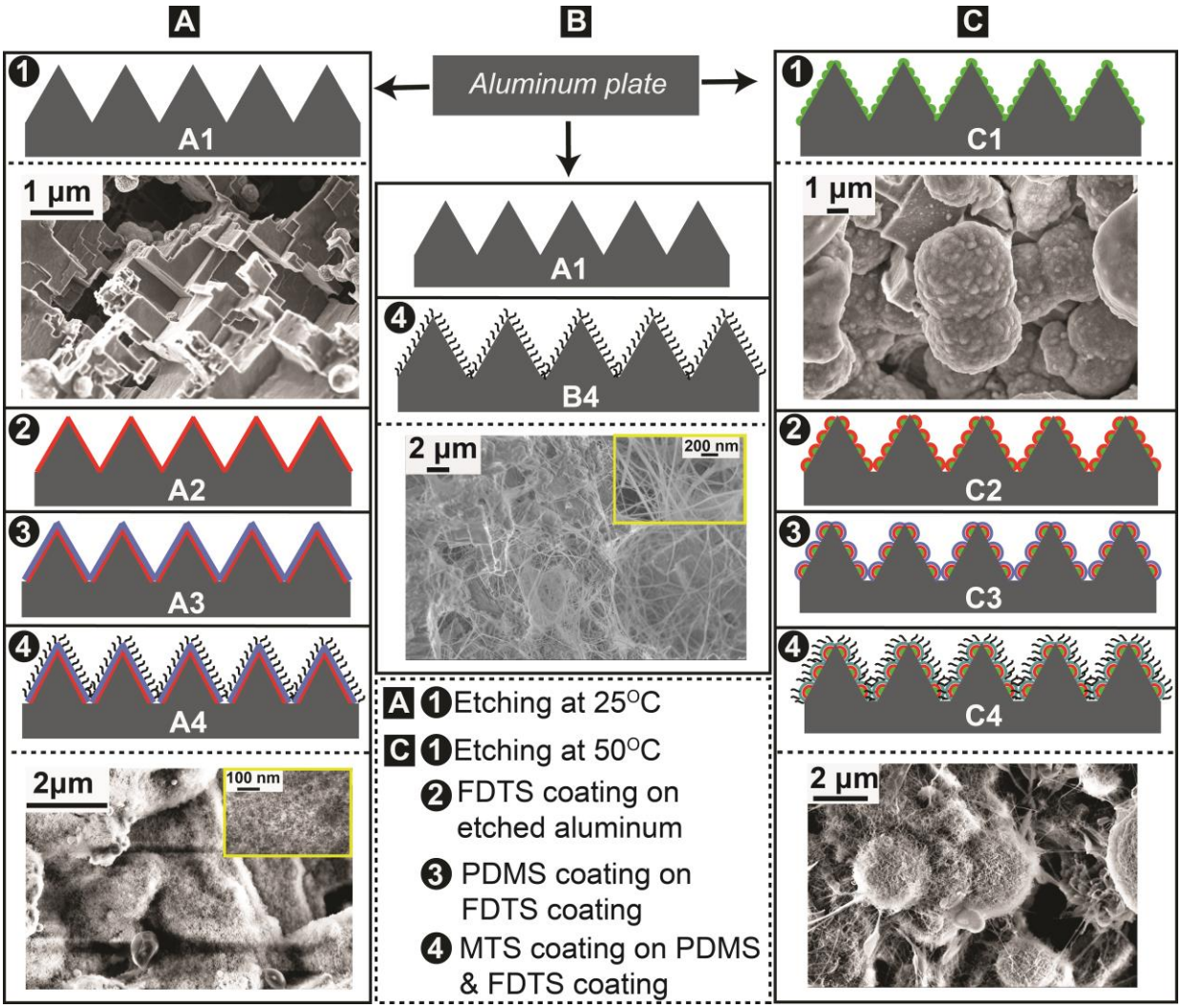

Fig. 2 Process schematic of fabrication of aluminum-based superhydrophobic surfaces. Processes A and C consist four different steps, which are labeled by numbers 1 through 4. In each step, one of the three different coatings are applied e.g. FDTS, PDMS and MTS nanofiber, which are depicted by a red line ( ), a blue line ( ) and black curls ( ) respectively. In process B, step 4 is imposed directly. SEM images show the resulting morphology for each process. In process C, the rounded features, depicted with green half circles ( ), denote the nanotextured microspherulites generated during etching at 50°C.

In addition to the SEM based morphological characterization, energy-dispersive X-ray spectroscopy (EDX) illustrated in Fig. 3was employed. The EDX spectra of the A1 surface confirmed that only aluminum was present, whereas the C1 surface spectrum demonstrates the presence of iron, which was seen to be prevalent in rounded microspherulites. The genesis of iron microspherulites can be explained by the fact that at higher temperature the sharp pits provide nucleation sites for iron which is produced from the chemical reaction (Equation 1 below) between the ferric chloride solution and the aluminum surface.

$$Al(s) + 3FeCl_3 \rightarrow 3FeCl_2 + AlCl_3 \quad (1)$$

This reaction is enhanced at higher temperatures and therefore the nucleation[33] of the iron on the sharp pits is also more probable on the C1 surface than on A1. As a result, the A1 surface only showed very dispersed microspherulites (see the SEM image of A1 in Fig. 2), whereas C1 was completely covered.

Nanoscale

RSCPublishing

ARTICLE

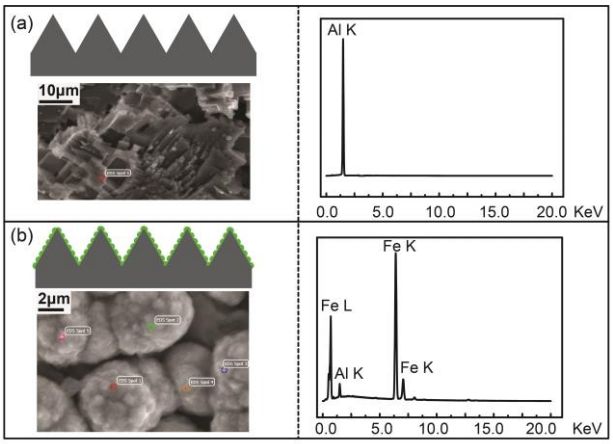

Fig. 3 The EDX spectra of two different surfaces, A1 and C1, obtained by aluminum etching with $FeCl_3$ solution at two different temperatures. The surface morphology obtained by etching the aluminum at (a) 25°C and (b) 50°C respectively. The EDX spectra are shown next to the schematic and the corresponding SEM image of the etched surface. The spots with different colors were highlighted to show the points where the EDX spectra were taken.

The presence of microspherulites on the top of pit walls has a clear effect on surface wetting at the macroscale, as reflected by the contact angle data of the intermediate A2 and C2 surfaces (coated by a monolayer of FDTS), which are illustrated in Fig. S1 in the Supplementary Information. The contact angle hysteresis of the C2 surface is only 2.7° ± 3.4°, which is significantly lower than that of A2 surface, at 29° ± 12°. The difference is attributed to the effect of rounded microspherulites: on the A2 surface, the sharp pit edges act as partial pinning locations for the contact line,[69] causing reduced θ_R and thus relatively high $\Delta\theta$. The presence of microspherulites on the sharp pit walls shadows the sharp edges, thereby decreasing the contact line pining, and thus, increasing θ_R and reducing $\Delta\theta$.

To impart a multi-scale hierarchical structure to the surface by adding nanoscale features, and to improve drop impact resistance, samples of MTS nanofibers were formed on the A4, B4 and C4 surfaces by immersion in an MTS solution in n-hexane for 12 hours. The θ_A, θ_R and $\Delta\theta$ measured on the three surfaces are shown in Fig. 4. It can be observed that the contact angle hysteresis was minimized on both A4 ($\Delta\theta$ =2.6°±3.6°) and C4 ($\Delta\theta$ =2.9°±4.6°) surfaces, due to the combined presence of FDTS/PDMS layers and MTS nanofibers. The hysteresis is slightly higher on B4 surfaces ($\Delta\theta$ =10.1°±6.9°), where only the MTS fibers are present on the pit walls. Overall, the A4, B4 and C4 surfaces show similar wetting properties with sessile drops, with almost identical θ_A ~160° and θ_R in the range of 150-160°. However, their robustness characteristics varied significantly, as will be shown below.

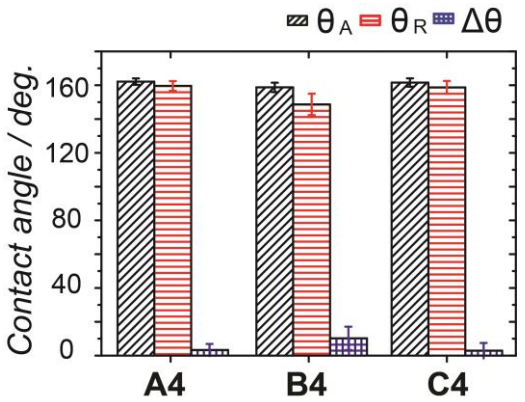

Fig. 4 The advancing, θ_A, and receding, θ_R, contact angles and the contact angle hysteresis, $\Delta\theta$, of three different surfaces: A4, B4 and C4.

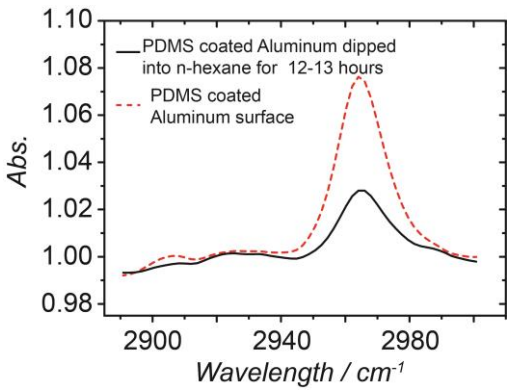

Fig. 5 The Fourier Transform Infrared (FTIR) spectra of PDMS coated smooth aluminum surface before (red dotted line) and after (black solid line) attack of n-hexane for 13 hours.

The MTS nanofibers were self-assembled from an n-hexane solution (see the Experimental Section below). Since n-hexane may cause delamination of PDMS over long exposures,[70] an FTIR study was performed on a PDMS coated aluminum sample, before and after dipping it into n-hexane for 13 hours, to check the eventual PDMS layer degradation. The FTIR spectra (see Fig. 5) confirmed partial degradation of PDMS layer after immersion into n-hexane, as the intensity of the peak of $\nu_{stretching}$ of $C-H$ (at 2960 cm^{-1}) was reduced compared to the fresh PDMS coated sample. Nonetheless, PDMS degradation was only partial and a thin PDMS thin layer was

Nanoscale RSCPublishing

ARTICLE

still present on the surface, as also confirmed by SEM images (see Fig. S2 in Supplementary Information), meaning that the MTS nanofiber fabrication step can be performed, without affecting the PDMS protective layer significantly.

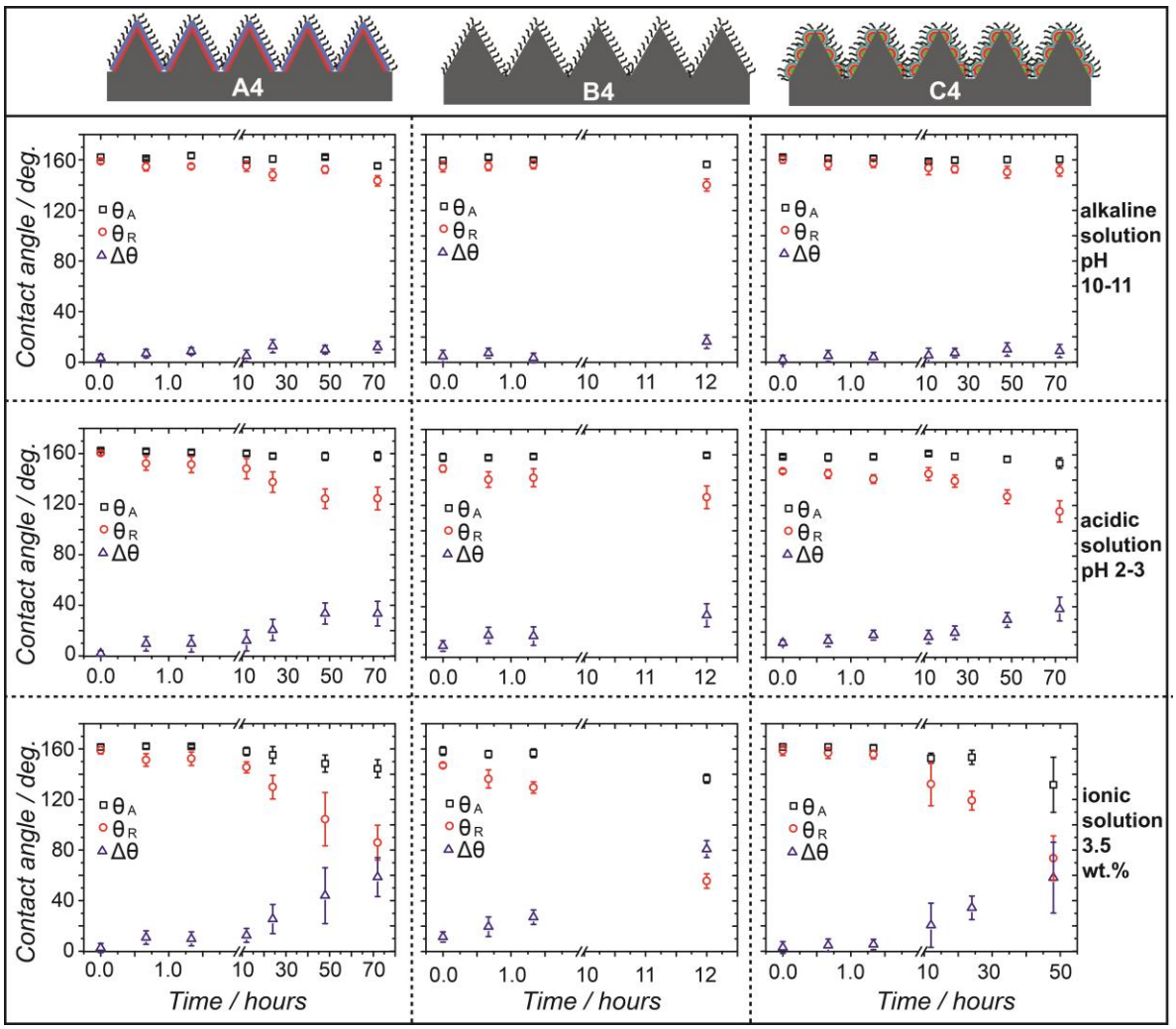

Fig. 6 Chemical stability tests on three different surfaces, A4, B4 and C4. The top most row shows the schematic of those surfaces (A4, B4 and C4 respectively). In the rows below the schematic, the chemical stability tests with alkaline (pH 10-11), acidic (pH 2-3) and ionic (3.5 % weight sodium chloride solution) solutions are shown, respectively. The pH of the acidic and alkaline water solutions were maintained constant by adding hydrochloric acid and sodium hydroxide solution, respectively.

Fig. 6 provides an overview of the chemical stability test for A4, B4 and C4 surfaces under three different chemical environments, i.e. acidic water (pH 2-3), alkaline water (pH 10-11) and ionic solution (3.5 weight % sodium chloride), the latter being representative of a corrosive environment like marine water. The surfaces were immersed into those solutions for several hours and periodically removed to monitor evolution of the wetting properties through contact angle measurement, as illustrated in Fig. 6. First, the results show that surfaces A4 and C4 were extremely stable in alkaline solution with pH of 10-11 and maintained a remarkable superhydrophobicity even after 72 hours ($\Delta\theta$ <10°), whereas the $\Delta\theta$ of surface B4 increased to 16° ± 5° already after only 12 hours

Nanoscale

RSCPublishing

ARTICLE

(note the different horizontal scales in the graphs). In the acidic solution of pH 2-3, A4 and C4 showed a similar behavior, with first signs of degradation after 24 hours, when the receding contact angle decreased down to ~140° and the contact angle hysteresis increased to ~20°, while the advancing contact angle remained approximately constant at ~160°. For the B4 surface, θ_A remained also constant, but a decrease of θ_R to 126° ± 9°, with consequent increase of $\Delta\theta$ to 33° ± 9° after 12 hours immersion suggests that a progressive degradation of the surface occurred much faster. These results also imply that θ_R and, as a consequence, $\Delta\theta$ provide a clearer indication of superhydrophobicity degradation compared to only θ_A, since θ_R is more sensitive to surface degradation than θ_A, which remains almost unaffected. Finally, after immersion of 72 hours in ionic solution, the receding contact angle of surface A4 reduces to a value below 120°, with the advancing contact angle remaining close to 150°. The resistance of the A4 surface is thus slightly better than that of the C4 surface, which completely degrades after 48 hours, with the value of θ_R becoming less than 90°. The resistance time to ionic solution of the surface B4 is again close to 12 hours, when $\Delta\theta$ =81° ± 9°.

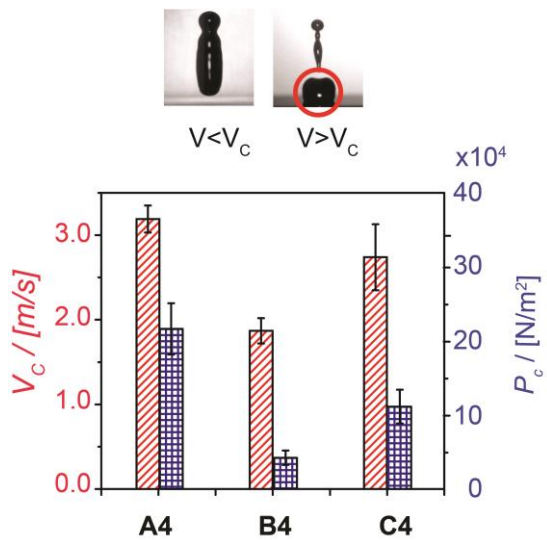

Fig. 7 Critical Velocity V_C and estimated capillary pressure P_C for three different surfaces A4, B4 and C4. In the image above the graph, it is shown that, if the impact velocity V is less than V_C, there is no water droplet portion left on the surface after the impact. On the other hand, if the impact velocity V is greater than V_C, there is an impaled drop remainder (highlighted with a red circle) after the impact as a consequence of liquid meniscus penetration.

The different behavior in chemical stability tests, between the A4, B4 and C4 surfaces can be explained by the role of different layers in the multilayer coatings. Indeed, FDTS and PDMS on A4 and C4 surface act as barrier layers; thus, A4 and C4 possess remarkably better stability than B4, which is only coated by MTS nanofibers. The small difference between A4 and C4 can be explained by differences in PDMS coating conformity. The more complex morphology on C-type surfaces, due to presence of rounded microspherulites (see SEM images in Fig. 2), should make it relatively harder to form a perfectly conformal PDMS coating compared to the A-type surfaces, where microspherulites are not present. The importance of PDMS as barrier layer was further confirmed by the study of the chemical stability of intermediate surfaces C2 and C3, presented in the Supplementary Information (see Fig. S3 in Supplementary Information): the C2 surface, coated with FDTS only, degrades within two hours in alkaline water or the ionic solution, whereas the stability of the C3 surface increases to up to two days, due to the presence of the PDMS as protective layer. The FDTS layer is nonetheless important to improve PDMS adhesion to the aluminum substrate.

To measure the surface resistance to the liquid meniscus penetration, drop impact tests were performed. Such tests allow to measure the value of the critical velocities, V_C, above which an impacting drop does not fully rebound from the surface and part of the drop remains attached (impaled). Impalement occurs when the pressure engendered during impact overcomes the resistive capillary pressure, P_C, which is directly proportional to the liquid surface tension, γ, to the advancing contact angle of water on a corresponding smooth surface, θ_A^s, and inversely proportional to the surface characteristic roughness, r, i.e. $P_C \propto \gamma \cos\theta_A^s / r$.[56] The exact formula for the capillary pressure can be derived *a priori* on simple, well defined geometries, such as micro-pillars or micro-grooves. However, on surfaces with random, hierarchical roughness, where multiscale structures are present, predicting the capillary pressure is more complex. Nonetheless, for such surfaces drop impact experiments can be used to indirectly measure the capillary pressure, P_C, from determination of the critical velocity, V_c, at which impalement occurs, as explained in reference 57[57] and in the Supplementary Information. The values of both V_c and estimated values of P_C are illustrated in Fig. 7. The best performing surface was A4, with a critical velocity of $V_c \approx$ 3.2±0.2 m/s, followed by C4 with $V_c \approx$ 2.7±0.2 m/s and B4 with $V_c \approx$ 1.9±0.2 m/s. The corresponding capillary pressure is 346 ± 34 kPa for the A4 surface, 111 ± 33 kPa for C4, and 42 ± 9 kPa for B4 (see calculation details in Supplementary Information). Note that even a relatively small variation of the drop impact critical velocity corresponds to a large

Nanoscale RSCPublishing

ARTICLE

variation in the surface capillary pressure, due to the fact that the developed pressure upon impact, which is needed to overcome the capillary pressure, scales with the impact velocity to approximately the power of three, $P_C \propto V^{28/9}$.[57] The large differences in drop impalement resistance can be understood with the help of the magnified SEM images of A4, B4 and C4 surfaces (see in Fig. 2). One of the main factors affecting meniscus penetration upon impact is the density of MTS fibers, which is controlled by the presence of $-OH$ groups on the substrate, serving as nucleation sites for nanofiber growth. The density of fibers on A4 and C4 surfaces was higher than on the B4 surface (see SEM images of B4 in Fig.8). In the case of B4 surface, $-OH$ groups were generated by treating the etched aluminum sample (B1) in oxygen plasma for 10 minutes, whereas for surfaces A4 and B4 the $-OH$ groups were generated on a PDMS thin film by immersion in boiling water and where thus denser.[71] With respect to the differences between A4 and C4, again they can be attributed to the PDMS layer: the PDMS film is more conformal on A4, so that MTS fiber distribution is more homogeneous on A4 than on C4.

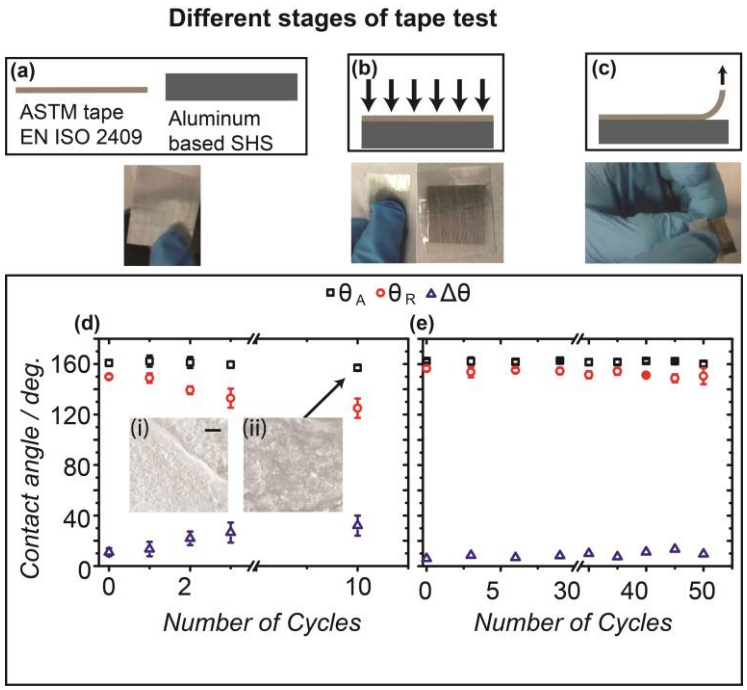

Fig. 8 The mechanical durability test on aluminum based superhydrophobic surfaces. Different steps performed are depicted in sequence in (a) to (c). Inside the graph (d) for surface A4, the SEM images before (i) and after (ii) 10 cycles of adhesion tape tests are shown. In (e), the contact angle evolution after tape tests on the surface C2 is shown (scale bar in SEM is 200 nm).

Finally, mechanical durability was tested on A4, since this was the best performing MTS coated surface from previous tests, together with the intermediate surface C2, i.e. the surface with only FDTS coating with very good wetting properties (low $\Delta\theta$). The ASTM standard adhesive tape (EN ISO 2409) was used for mechanical peel test.[64] As described in Fig. 8a-c, the tests consisted of (a) tape application on the sample (b) pressing and rubbing to ensure best tape adhesion and (c) tape peel off from the sample. On the A4 surface, after 10 cycles, the advancing contact angle was still high, at ~160°, but the receding contact angle decreased to ~120°, with contact angle hysteresis increasing up to 40°. The SEM image in Fig. 8 shows that degradation of the surface was caused by peeling of the nanofibers. On the other hand, the C2 surface preserves its exceptional superhydrophobicity even after 50 cycles of tape tests: both advancing and receding contact angles remain high, with $\Delta\theta$ remaining lower than 10^o. This shows that the C2 surface, despite having a lower chemical stability, with a degradation of the sample within two hours when immersed into a solution of alkaline

Nanoscale

RSCPublishing

ARTICLE

water with pH 10-11 and in ionic solution (see Fig. S3 in Supplementary Information), could be suitable for applications where mechanical durability is a priority. The good mechanical properties of C2 are guaranteed by a combination of hierarchical surface structuring, offered by pits and microspherulites, and functionalization by FDTS, which is grafted chemically onto the surface and thus adheres more robustly to the substrate.

In order to provide a global overview, the studies of chemical durability, drop meniscus impalement resistance and mechanical durability of all surfaces are listed in the Table 1. The color codes are used to designate the relative performance, such as green: good, yellow: acceptable, red: poor.

were tested not only for their water repellency with static contact angle measurements and drop impact tests, but also for their robustness including chemical stability in acid, alkaline and corrosive ionic solutions and mechanical stability using tape peel tests. The surface design and development were based on the control of the micro and nanoscale morphology, through environmentally benign aluminum etching with iron chloride, in combination with single or multiple hydrophobic layers, including a self-assembled FDTS monolayer, PDMS thin film, MTS nanofibers. Results proved that combined use of multiple layers, i.e. FDTS and PDMS, conferred optimal chemical stability properties to the superhydrophobic surface, which were capable of resisting up to 72 hours in severely adverse environments.

Table 1. Performance evaluation of different surfaces: Colour code: green: good, yellow: acceptable, red: poor.

Surfaces	Wetting Performance ($\Delta\theta$, ^{o})	Chemical stability	Drop impalement resistance (V_C, m/s)	Mechanical durability (No. of cycles)
A2	29±12	--	--	--
A3	30±11	--	--	--
A4	2.6±3.6	~ 72 hours (for alkali and acidic solution) ~ 48 hours (for ionic solution)	3.2±0.2	10
B4	10.1±6.9		1.87±0.1	--
C2	2.7±3.4	~ 2hr	1.86±0.4	50
C3	4.1±4.2		1.87±0.2	--
C4	2.9±4.6		2.74±0.4	--

Conclusion

In closing, our work aimed at identifying a rational framework for the development and fabrication of robust, hierarchically nanotextured superhydrophobic surfaces on aluminum. The surfaces

The layer of MTS nanofibers imparted additional hierarchical structuring introducing nanoscale features, which led to minimization of contact angle hysteresis and to an increase in

Nanoscale

RSCPublishing

ARTICLE

surface capillary pressure, improving liquid meniscus penetration resistance. On the other hand, maximization of surface mechanical durability was achieved on surfaces with microscale roughness functionalized by self-assembly of FDTS, without the nanofiber layer, since molecular grafting to the oxidized aluminum substrate guarantees high adhesion of the layer to the substrate, compared to films and nanofibers. The FDTS coated surface showed impressive mechanical durability, being able to resist 50 cycles of tape peel tests, without deterioration of surface superhydrophobicity ($\Delta\theta < 10^{\circ}$).

Experimental

Surface and Chemicals

The aluminum substrate (AW 1085) having composition of (Al 99.85%, Si 0.1%, Fe 0.12%, Cu 0.03%, Mn 0.02%, Mg 0.02%, Zn 0.03%, Ti 0.02%, Ga 0.03% and V 0.05%) was purchased from Metall Service Menziken AG. Acetone, isopropyl alcohol, n-hexane, tetrahydrofuran (THF) and methyltrichlorosilane (99%) were purchased from Sigma Aldrich and were used without further purification. Anhydrous ferric chloride (reagent grade, 97%) and sodium hydroxide pellets (<98%, anhydrous) were also purchased from Sigma Aldrich. 1H,1H,2H,2H-Perfluorodecyltrichlorosilane (FDTS) $C_{10}H_4Cl_3F_{17}Si$ was purchased from Alfa Aesar. The deionized (DI) water (18.2 MΩ, Mill-Q pore) was used for contact angle measurements and drop impact experiments. Polydimethylsiloxane (PDMS) based elastomer was purchased as Sylgard 184® silicon elastomer kit from Dow Corning.

Surface preparation

The different process schematics (Fig. 2) described the fabrication of aluminum based superhydrophobic surfaces. Three different processes, labelled as A, B and C, were used. In processes A and C, there are 4 steps, (see Fig. 2). Process B consisted of two steps (1 and 4). The aluminum substrates (size 2cm x 2cm) were initially cleaned under sonication in acetone, isopropyl alcohol and deionized water for 10 minutes each. To prepare the samples and remove native oxide layer, cleaned samples were also treated with 1 weight% sodium hydroxide solution for 10 minutes under ultrasonication and then cleaned again with deionized water. Subsequently, the aluminum surface was etched with 1 (M) ferric chloride solution for 25 minutes with probe sonication (power, amplitude 80%). During etching with ferric chloride solution (step #1 in Fig. 2), the aluminum samples were cleaned every 2.5 minutes with isopropyl alcohol for 2-3 minutes to avoid precipitation of ferric hydroxide on the surface. The etching was performed at two different temperatures, i.e. at 25°C (for processes A and B) and at 50°C (for process C). In the step #2 (processes A and C), the samples were treated with 1.43 m(M) solution of trichloro-1H, 1H, 2H, 2H-perflurodecylsilane (FDTS) in n-hexane solution for two hours, to impart hydrophobicity, and then baked for 45 minutes at 120°C. During step #3 (process A and C), a PDMS layer was formed using a solution of PDMS in THF. The solution was prepared by mixing 70 mg of Sylgard 184® and 7 mg of curing agent in 50 ml of THF, in a custom made dip coating unit. Right after the coating with PDMS, the surface was baked at 130°C for 30 minutes. In order to prepare the samples for step #4, the A3 and C3 surfaces were treated in boiling water for 5 minutes for hydrolysis reaction, which generates $-OH$ groups on the PDMS surface[7171]. The formation of $-OH$ group is needed for the following fiber coating process (step #4). In process B, the bare aluminum etched samples were treated with oxygen plasma for 10 minutes at 100 W, to generate $-OH$ groups. Finally, during step #4 the samples were dipped into a 0.14 (M) solution of methyltrichlorosilane (MTS) in n-hexane for 12 hours. At the end, the surface was rinsed in n-hexane for five minutes and baked at 100°C (processes A and C) or at 120°C (process B) for 30 minutes.

Surface characterization

The surface morphologies were studied by scanning electron microscopy (Zeiss ULTRA 55). The EDX study was performed by EDAX (TEAM™ EDS analysis). The Fourier Transform Infrared (FTIR) spectroscopy was performed by Vertex 80/80V (Bruker).

Contact angle measurements

An in-house goniometer system was used. The system consisted of a zoom lens (Thorlabs, MVL7000) fitted to a CCD camera. A syringe pump (Harvard Instruments) was employed for altering the volume of drops on the surfaces thereby enabling measurement of the advancing and receding contact angles, as well as the contact angle hysteresis.

Drop impact experiment

A high-speed camera (Phantom V9.1) was used to record the drop impact at the rate of 2500 frames per second. DI water drops of 2.2 mm diameter were generated using a fine needle fitted to a syringe pump (PHD Ultra, Harvard Apparatus).

Adhesion tape test

The mechanical durability was evaluated by ASTM standard adhesion tape test (ASTM EN ISO 2409).

Nanoscale

RSCPublishing

ARTICLE

Acknowledgements

Funding from Swiss National Science Foundation (SNF) grant 200021_135479 is gratefully acknowledged. CA acknowledges funding through a Marie Curie Intra-European Fellowship within the 7th FP of European Community (ICE^2, 301174). The authors thank Dr. Vikrant Vijay Naik for his help with the FTIR study.

Notes and References

[a]*Laboratory of Thermodynamics in Emerging Technologies, Mechanical and Process Engineering Department, ETH Zurich, 8092 Zurich, Switzerland. E-mail: dimos.poulikakos@ethz.ch.*

[ζ]*Current address: Mechanical Engineering, University College of London, Torrington Place, London, WC1E 7JE.*

† Electronic Supplementary Information (ESI) available: Contact angles on intermediate surfaces; PDMS film thickness change with n-hexane immersion; Chemical stability of surfaces with (C3) and without PDMS film (C2) and Impalement pressure balance. See DOI: 10.1039/b000000x/

1. S. Jung, M. Dorrestijn, D. Raps, A. Das, C. M. Megaridis and D. Poulikakos, *Langmuir*, 2011, 27, 3059-3066.

2. C. Antonini, M. Innocenti, T. Horn, M. Marengo and A. Amirfazli, *Cold Reg. Sci. Technol.*, 2011, 67, 58-67.

3. L. Cao, A. K. Jones, V. K. Sikka, J. Wu and D. Gao, *Langmuir*, 2009, 25, 12444-12448.

4. S. Jung, M. K. Tiwari, N. V. Doan and D. Poulikakos, *Nat. Commun.*, 2012, 3.

5. S. Tarquini, C. Antonini, A. Amirfazli, M. Marengo and J. Palacios, *Cold Reg. Sci. Technol.*, 2014, 100, 50-58.

6. A. Asatekin, S. Kang, M. Elimelech and A. M. Mayes, *J. Membrane Sci.*, 2007, 298, 136-146.

7. N. Min, P. Patel, S. Kai and D. D. Meng, *2009 4th IEEE International Conference on Nano/Micro Engineered and Molecular Systems (IEEE-NEMS 2009)*, 2009, DOI: 10.1109/nems.2009.5068746, 1017-1020.

8. Y. Bo, F. Liang, T. An-qiong, H. Qiu-liu, H. Jia, M. Jian-hui, B. Ge and B. Huan, *Appl. Surf. Sci.*, 2011, 258, 580-585.

9. D. Torresin, M. K. Tiwari, D. Del Col and D. Poulikakos, *Langmuir*, 2013, 29, 840-848.

10. R. Hensel, A. Finn, R. Helbig, H. G. Braun, C. Neinhuis, W. J. Fischer and C. Werner, *Adv. Mater.*, 2013.

11. H. Bellanger, T. Darmanin, E. Taffin de Givenchy and F. d. r. Guittard, *Chem. Rev.*, 2014.

12. W. Li and A. Amirfazli, *Ad . Colloid. Interface Sci.*, 2007, 132, 51-68.

13. W. Li and A. Amirfazli, *Soft Matter*, 2008, 4, 462.

14. L. Jiang, Y. Zhao and J. Zhai, *Angew. Chem-Ger Edit*, 2004, 116, 4.

15. J. Liu, Y. Cai, X. Wang, B. Ding and M. Wang, *Nanoscale*, 2011, 3, 5.

16. R. Asmatulu, M. Ceylan and N. Nuraje, *Langmuir*, 2010, 27, 4.

17. C. S. Sharma, A. Sharma and M. Madou, *Langmuir*, 2010, 26, 2218-2222.

18. E. Mele, I. S. Bayer, G. Nanni, J. A. Heredia-Guerrero, R. Ruffilli, F. Ayadi, L. Marini, R. Cingolani and A. Athanassiou, *Langmuir*, 2014, DOI: 10.1021/la4048177.

19. A. Hozumi and T. J. McCarthy, *Langmuir*, 2010, 26, 7.

20. K. Liu, J. Zhai and L. Jiang, *Nanotechnology*, 2008, 19, 6.

21. Z. Guo, X. Chen, J. Li, J.-H. Liu and X.-J. Huang, *Langmuir*, 2011, 27, 8.

22. K. Zhao, K. S. Liu, J. F. Li, W. H. Wanga and L. Jiang, *Scripta. Mater.*, 2009, 60, 3.

23. Y. Xiu, Y. Liu, D. W. Hess and C. P. Wong, *Nanotechnology*, 2010, 21, 5.

24. Z. Guo, F. Zhou, J. Hao and W. Liu, *J. Am.Chem. Soc.*, 2005, 127, 2.

25. T.I. Kim, D. Tahk and H. H. Lee, *Langmuir*, 2009, 25, 4.

26. C. Gu, H. Ren, J. Tu and T.-Y. Zhang, *Langmuir*, 2009, 25, 9.

27. D. Qi, N. Lu, H. Xu, B. Yang, C. Huang, M. Xu, L. Gao, Z. Wang and L. Chi, *Langmuir*, 2009, 25, 6.

28. F. Mumm, A. T. J. van Helvoort and P. Sikorski, *ACS Nano*, 2009, 3, 6.

29. D. Xie and W. Li, *Appl. Surf. Sci.*, 2011, 258, 4.

30. L. Liu, J. Zhao, Y. Zhang, F. Zhao and Y. Zhang, *J. Colloid. Interface Sci.*, 2011, 358, 277-283.

31. N. Saleema, D. K. Sarkar, D. Gallant, R. W. Paynter and X. G. Chen, *ACS Appl. Mater. Interfaces*, 2011, 3, 4775-4781.

32. N. Saleema, D. K. Sarkar, R. W. Paynter and X. G. Chen, *ACS Appl. Mater. Interfaces*, 2010, 2, 2500-2502.

Nanoscale

RSCPublishing

ARTICLE

33. Z. Ying, W. Meng, L. Xin and H. Weidong, *J. Mater. Sci. Technol.*, 2012, 28, 67-72.

34. L. Liu, F. Xu and L. Ma, *J. Phys. Chem. C*, 2012, 116, 6.

35. X. Hou, F. Zhou, B. Yu and W. Liu, *Mater. Sci. Eng. A*, 2007, 452-453, 5.

36. H.-J. Oh, J.-H. Lee, H.-J. Ahn, Y. Jeong, N.-J. Park, S.-S. Kim and C.-S. Chi, *Mater. Sci. Eng.*, 2007, A 449-451, 4.

37. O. Cakır, *J. Mater. Process. Tech.*, 2008, 199, 4.

38. M. Nosonovsky, V. Hejazi, A. E. Nyong and P. K. Rohatgi, *Langmuir*, 2011, 27, 14419-14424.

39. S. Naha, S. Sen and I. K. Puri, *Carbon*, 2007, 45, 1702-1706.

40. M. K. Tiwari, I. S. Bayer, G. M. Jursich, T. M. Schutzius and C. M. Megaridis, *ACS Appl. Mater. Interfaces*, 2010, 2, 1114-1119.

41. B. Cortese, S. D'Amone, M. Manca, I. Viola, R. Cingolani and G. Gigli, *Langmuir*, 2008, 24, 2712-2718.

42. C. Zhijun, G. Yabing and F. Shaoming, *Surf. Interface Anal.*, 2010, 42, 1-6.

43. P. Roach, N. J. Shirtcliffe and M. I. Newton, *Soft Matter*, 2008, 4, 224-240.

44. Y. Zhang, X. Yu, H. Wu and J. Wu, *Appl. Surf. Sci.*, 2012, 258, 8253-8257.

45. Q. F. Xu and J. N. Wang, *New J. Chem.*, 2009, 33, 734-738.

46. L. Shixiang, C. Yiling, X. Wenguo and L. Wei, *Appl. Surf. Sci.*, 2010, 256, 6072-6075.

47. F. Wang, C. Li, Y. Lv, F. Lv and Y. Du, *Cold Reg. Sci. Technol.*, 2010, 62, 29-33.

48. S. Ji, P. A. Ramadhianti, N. Thanh-Binh, W.-d. Kim and H. Lim, *Microelectron. Eng.*, 2013, 111, 404-408.

49. H. Cho, D. Kim, C. Lee and W. Hwang, *Curr. Appl. Phys.*, 2013, 13, 762-767.

50. Y. Liu, J. Liu, S. Li, J. Liu, Z. Han and L. Ren, *ACS Appl. Mater. Interfaces*, 2013, 5, 8.

51. M. Ruan, W. Li, B. Wang, B. Deng, F. Ma and Z. Yu, *Langmuir*, 2013, 29, 8482-8491.

52. C. Antonini, F. J. Carmona, E. Pierce, M. Marengo and A. Amirfazil, *Langmuir*, 2009, 25, 6143-6154.

53. D. Quere, *Rep. Prog. Phys.*, 2005, 68, 2495-2532.

54. C. Antonini, F. Villa, I. Bernagozzi, A. Amirfazli and M. Marengo, *Langmuir*, 2013, 29, 16045-16050.

55. M. Reyssat, A. Pepin, F. Marty, Y. Chen and D. Quere, *Europhys. Lett.*, 2006, 74, 306-312.

56. D. Bartolo, F. Bouamrirene, E. Verneuil, A. Buguin, P. Silberzan and S. Moulinet, *Europhys. Lett.*, 2006, 74, 299-305.

57. T. Maitra, M. K. Tiwari, C. Antonini, P. Schoch, S. Jung, P. Eberle and D. Poulikakos, *Nano Lett.*, 2014, 14, 172-182.

58. X. Deng, L. Mammen, Y. Zhao, P. Lellig, K. Muellen, C. Li, H. J. Butt and D. Vollmer, *Adv. Mater.*, 2011, 23, 2962-2965.

59. T. Verho, C. Bower, P. Andrew, S. Franssila, O. Ikkala and R. H. A. Ras, *Adv. Mater.*, 2011, 23, 673-678.

60. D. Xu, L. Mammen, H. J. Butt and D. Vollmer, *Science*, 2012, 335, 67-70.

61. D. M. Allen and P. Jefferies, *CIRP Ann. Manuf. Technol.*, 2006, 55, 4.

62. B. Qian and Z. Shen, *Langmuir*, 2005, 21, 3.

63. L. Gao and T. J. McCarthy, *J. Am. Chem. Soc.*, 2006, 128, 9052-9053.

64. R. Menini and M. Farzaneh, *Surf. Coat. Tech.*, 2009, 203, 1941-1946.

65. D. Quere, M. J. Azzopardi and L. Delattre, *Langmuir*, 1998, 14, 2213-2216.

66. E. Pierce, F. J. Carmona and A. Amirfazli, *Colloid Surface A*, 2008, 323, 73-82.

67. W. Li and A. Amirfazli, *J. Colloid Interface Sci.*, 2005, 292, 195-201.

68. W. Barthlott and C. Neinhuis, *Planta*, 1997, 202, 1-8.

69. A. T. Paxson and K. K. Varanasi, *Nat. Commun.*, 2013, 4.

70. J. N. Lee, C. Park and G. M. Whitesides, *Anal. Chem.*, 2003, 75, 6544-6554.

71. P. Joong Yull, A. Dongchan, C. Yoon Young, H. Chang Mo, S. Takayama, L. Soon Hyuck and L. Sang-Hoon, *Sense. Actuator B-Chem.*, 2012, 173, 765-771.